Ferroelectric Phase Diagram of PVDF:PMMA

Mengyuan Li,*[,†] Natalie Stingelin,[⊥,‖] Jasper J. Michels,[§] Mark-Jan Spijkman,[†] Kamal Asadi,[‡] Kirill Feldman,[○] Paul W. M. Blom,[†,§] and Dago M. de Leeuw[†,‡]

[†]Zernike Institute for Advanced Materials, University of Groningen, Nijenborgh 4, 9747 AG, Groningen, The Netherlands

[‡]High Tech Campus 4, Philips Research Laboratories, 5656AE, Eindhoven, The Netherlands

[§]High Tech Campus 31, Holst Centre, 5605 KN Eindhoven, The Netherlands

[⊥]Department of Materials and Centre for Plastic Electronics, Imperial College London, Exhibition Road, London, SW7 2AZ, U.K.

[‖]FRIAS, School of Soft Matter Research, University of Freiburg, 79104 Freiburg, Germany

[○]Department of Materials, Eidgenössische Technische Hochschule (ETH) Zürich, Wolfgang-Pauli Strasse CH-8093 Zürich, Switzerland

ABSTRACT: We have investigated the ferroelectric phase diagram of poly(vinylidene fluoride) (PVDF) and poly(methyl methacrylate) (PMMA). The binary nonequilibrium temperature composition diagram was determined and melting of α- and β-phase PVDF was identified. Ferroelectric β-PVDF:PMMA blend films were made by melting, ice quenching, and subsequent annealing above the glass transition temperature of PMMA, close to the melting temperature of PVDF. Addition of PMMA suppresses the crystallization of PVDF and, as a consequence, the roughness of blend films was found to decrease with increasing PMMA content. Using time-dependent 2D numerical simulations based on a phase−field model, we qualitatively reproduced the effect of PMMA on the crystallization rate and the spherulite shape of PVDF. The remnant polarization scaled with the degree of crystallinity of PVDF. The thermal stability of the polarization is directly related to the Curie temperature. We show that, at high temperature, the commodity ferroelectric PVDF:PMMA blends outperform the commonly employed specialty copolymer poly(vinylidene fluoride−trifluoroethylene) (P(VDF−TrFE)).
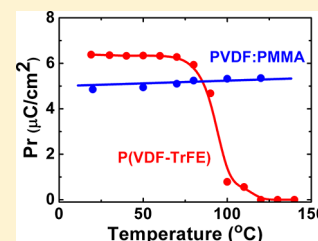
1. INTRODUCTION

Ferroelectric polymers are ideal candidates for data storage applications as they exhibit an intrinsic bistable, remnant polarization that can repeatedly be switched by an electric field.[1] Memories based on capacitors,[2] field-effect transistors,[3,4] and ferroelectric-blend diodes[5−7] have been reported. The most commonly used macromolecular ferroelectric is the random copolymer poly(vinylidene fluoride-trifluoroethylene) (P-(VDF−TrFE)). Its chemical structure is presented in the inset of Figure 1. This copolymer is widely applied for its ease of processing; thin films can be made from solution by spin-coating, wire-bar coating[8] and patterned by, e.g., nanoembossing.[9] In comparison to other organic ferroelectrics, the copolymer P(VDF−TrFE) exhibits advantageous properties such as a relatively large remnant polarization, low leakage currents due to a high electrical resistivity and switching times as short as 1 μs. However, large-scale integration of P(VDF−TrFE) in ferroelectric devices is hampered by the limited thermal stability of the remnant polarization due to its low Curie temperature, the relative large surface roughness of ferroelectric films and the stack integrity.

First, to demonstrate the limited thermal budget we fabricated capacitors with P(VDF−TrFE) (65−35 mol %). The remnant polarization as a function of temperature is presented in Figure 1. At room temperature the polarization is about 7 μC/cm^2 in good agreement with literature data.[10,11] However, already at 50 °C, the polarization decreases notably and rapidly deteriorates at more elevated temperatures. This limited thermal stability[12−14] is

due to the low Curie temperature of P(VDF−TrFE) which, of course, severely hampers applications at higher temperatures.

Second, the coercive field of P(VDF−TrFE) is about 50 MV/m. To achieve operation at low voltage, the ferroelectric film should be as thin as possible. As-deposited thin films are typically amorphous, and in order to generate the ferroelectric phase, the films have to be annealed above the Curie temperature. This annealing protocol causes crystal growth and an increase in surface roughness, which for very thin films may hamper the yield of ferroelectric capacitors, and which deteriorates the charge carrier mobility in ferroelectric field-effect transistors.

Finally, P(VDF−TrFE) is soluble in common organic solvents which encumbers the stack integrity of multilayer devices such as field-effect transistors. Hence, upon spin coating an organic semiconductor, the already deposited P(VDF−TrFE) film may dissolve. Orthogonal solvents to substantially prevent intermixing are not readily available.

An alternative ferroelectric polymer that may provide improved thermal stability and multilayer stack integrity is the homopolymer poly(vinylidene fluoride) (PVDF). Neat PVDF films, however, cannot be applied as thin films generally crystallize in the paraelectric α-phase. Recently, blend films of PVDF and poly(methyl methacrylate) (PMMA) have been investigated for their ferroelectric properties and application as

energy storage medium.[15,16] Also, a method to fabricate ferroelectric PVDF films with low surface roughness has recently been reported.[17] PVDF:PMMA blend films were spin coated and after melting quenched in ice water. The amorphous films thus produced were subsequently annealed for 2 h at 150 °C. The PMMA retards the crystallization of PVDF yielding nanocrystalline β-phase PVDF crystals and smooth ferroelectric films. The polarization was found to monotonically decrease with PMMA content. A polarization of 4 μC/cm^2 was reported when using 20 wt % PMMA.
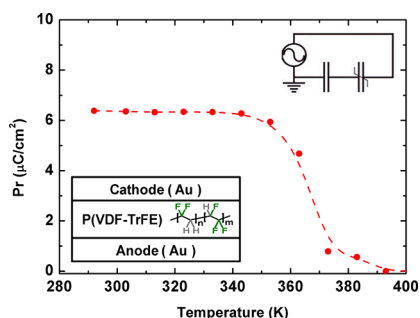

Figure 1. Remnant polarization, P_r, of ferroelectric capacitors based on the random copolymer poly(vinylidene fluoride-trifluoroethylene) (P(VDF−TrFE)) (65−35 mol %) as a function of temperature. The inset presents the capacitor layout with the chemical structure of P(VDF−TrFE) and the Sawyer−Tower circuit used for the measurement. The solid line is a guide to the eye.

Here we investigate in depth the blend films of PVDF:PMMA. We varied the molecular weight of the PMMA, the blend composition and the processing conditions. The phase identification and microstructure of the films was investigated by X-ray diffraction (XRD), Fourier-transform infrared microscopy (FTIR) and atomic force microscopy (AFM). We find that the solidification behavior and the film roughness correlate with the phase diagram, determined in this work. The time and temperature evolution of the topology have been reproduced by 2D numerical calculations using a phase-field model. The displacement current as a function of bias is measured in capacitors. The reported polarization and surface roughness[17] could be reproduced. In an assessment of the thermal stability we demonstrate that blending of PVDF with PMMA leads to smooth ferroelectric thin films that outperform the standard P(VDF−TrFE) films at high temperature.

2. PHASE DIAGRAM OF PVDF−PMMA

Polymer blends, due to their long-chain nature, generally phase separate. Miscibility between polymers can, however, be promoted by dipole or van der Waals interactions and hydrogen bonding. The monomeric unit of PVDF has a large electric dipole moment, and it is therefore not surprising that PVDF is miscible with a number of polymers which also exhibit a large dipole moment, such as poly(methyl methacrylate), poly(vinyl acetate) and poly(tetramethylene adipate). Blends of PVDF:PMMA have been the standard system for the study of mixing of polymers because of its availability and interesting structural and thermodynamic phenomena occurring in a thermally accessible temperature range. These blends are miscible and thermodynamically stable at all compositions due to the dipole/dipole interaction between the >CF$_2$ groups of PVDF and the >C=O groups of PMMA and to the hydrogen bonding between the double bonded oxygen of the carbonyl group and the acidic

hydrogen of the −CH$_2$−CF$_2$− group.[18,19] A review of PVDF and its blends has been reported by Jungnickel.[20]

We constructed the PVDF:PMMA temperature/composition (phase) diagram from differential scanning calorimetry (DSC) first-heating thermograms using PVDF with a molecular weight of 180 kg/mol and PMMA of 91 kg/mol. The binary nonequilibrium diagram is presented in Figure 2. Similar data
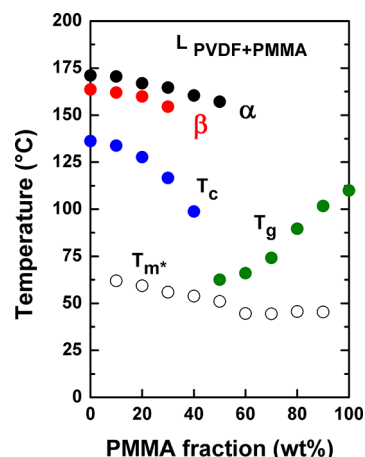

Figure 2. Binary nonequilibrium temperature/composition diagram of PVDF:PMMA as obtained for melt-extruded blends. The diagram was constructed with peak melting transition temperatures of PVDF recorded during the first heating scan in differential scanning calorimetry. Black and red circles represent melting of the α-PVDF and β-PVDF respectively. The blue circles correspond to the exothermic recrystallization temperature, T_c, of PVDF upon cooling. The glass transition temperature, T_g, is shown in green. The open circles, T_{m*}, represent a very weak low-temperature endothermic peak, which has previously been ascribed to melting of some small, imperfect PVDF crystallites,[20,21,26] typically disappears in a DSC second heating scan.

were obtained for melt-extruded blends and films cast from DMF. The diagram in Figure 2 is in good agreement with those earlier reported.[20,21] The melting point of PVDF and a single glass transition temperature of PVDF:PMMA that both monotonically change with composition, confirm that PVDF and PMMA are miscible over the entire composition range both in the melt and when quenched into a vitreous solid solution.

The thermogram of neat α-PVDF shows a single melting peak at 166 °C. With increasing PMMA content a second melting peak at slightly lower temperature is observed. We ascribe the additional melting peak to the presence of β-PVDF, based on a combined FTIR, electron diffraction and DSC investigation on highly oriented neat PVDF films that has shown that these two peaks can be ascribed to melting of the α-phase and β-phase of PVDF.[22] We confirmed this identification with DSC measurements on neat α-PVDF and on neat β-PVDF prepared by drawing a PVDF film at 70 °C to a draw ratio of 6. The melting points of both phases are reported to be depressed upon addition of PMMA.[23] In the diagram, we also have included the recrystallization temperatures of PVDF upon cooling (solid, blue circles). For blends comprising 40 wt % PMMA or more, PVDF does not recrystallize and the films remain amorphous. The open circles represent a very weak low-temperature endothermic peak, which has previously been ascribed to melting of some small, imperfect PVDF crystallites.[24,25] This peak disappears in the second heating.[26]

We note that the Curie temperature of neat PVDF has not yet unambiguously been identified. However, thermograms of the

commonly used random copolymer P(VDF−TrFE) show a ferroelectric-paraelectric transition depending on composition. The Curie temperature increases with increasing VDF content. Extrapolation then suggests that the Curie temperature of neat PVDF is about 172 °C.[27] In the DSC measurements of the PVDF:PMMA blends we could not detect any feature that could be ascribed to the Curie temperature of PVDF, which suggests that the Curie temperature of the blends is higher than the melting temperature.

3. MICROSTRUCTURE AND PHASE IDENTIFICATION OF THIN BLEND FILMS

Further information on the PVDF:PMMA microstructure development was obtained from wide-angle X-ray diffraction measurements. As-cast blend films were found to be amorphous.

In a first set of experiments, these films were molten and slowly cooled down to room temperature. XRD measurements showed that at blend compositions of up to about 40 wt % of PMMA, PVDF crystallizes in the α-phase. At higher PMMA content the films remain amorphous. The presence of such a large amount of PMMA completely suppresses the crystallization of PVDF, in agreement with the phase diagram. In order to induce the ferroelectric β-phase, in a second series of trials, the blend films were molten and quenched in ice water. These fully amorphous films were subsequently annealed. For blends comprising 10−30 wt % PMMA, predominantly the β-phase is obtained. The degree of crystallinity increases with annealing temperature. The optimum temperature is around 140−150 °C, i.e., slightly below the melting temperature of PVDF. As a typical example, XRD diffractograms of PVDF:PMMA (70:30) blend films are presented in Figure 3a. The molten and slowly cooled blend film crystallizes in the α-phase characterized by strong peaks at diffraction angles 2θ of 17.6° and of 20°, assigned to the (100) and (110) reflections, respectively.[28] The film melted, ice quenched and subsequently annealed at 140 °C, crystallizes in the β-phase as indicated by a diffraction peak at 2θ of 20.7°, corresponding to the overlapping (110) and (200) reflections.[28]

The phase identification was corroborated by FTIR measurements. The corresponding spectra are presented in Figure 3b. The α-phase of PVDF exhibits a trans−gauche (TGTG′) conformation which is characterized by characteristic absorption bands at 764, 795, 855, and 976 cm^{-1}, while the all-trans (TTTT) conformation of the β-phase of PVDF features characteristic absorption peaks at 840 and 1279 cm^{-1}.[29]

The amorphous PMMA apparently hinders the α-crystallization and promotes the β-phase formation. The reason might be related to the difference in crystal structures. For steric reasons the dipole/dipole interactions favor the trans-conformation of the highly polar β-PVDF polymorph over the trans−gauche conformation of the nonpolar α-PVDF. We note that the microstructure of many polymer blend films typically depends on the molecular weight of the components. However, as shown in Table 1, when we varied the molecular weight of PMMA, invariably the PVDF β-phase was obtained in blends comprising 10 wt % of PMMA and more, irrespective of the molecular weight of the PMMA. The origin is not yet understood.

AFM measurements on thin films of neat PVDF showed the typical spherulites[30] with sizes in the order of 10 to 100 μm. The thin films exhibit a surface roughness in the order of 10 nm. The roughness is reduced upon blending with PMMA. Typical AFM images of molten, ice quenched and annealed films as a function of composition are presented in Figure 4. The images show that with increasing PMMA content, the PVDF crystal growth is
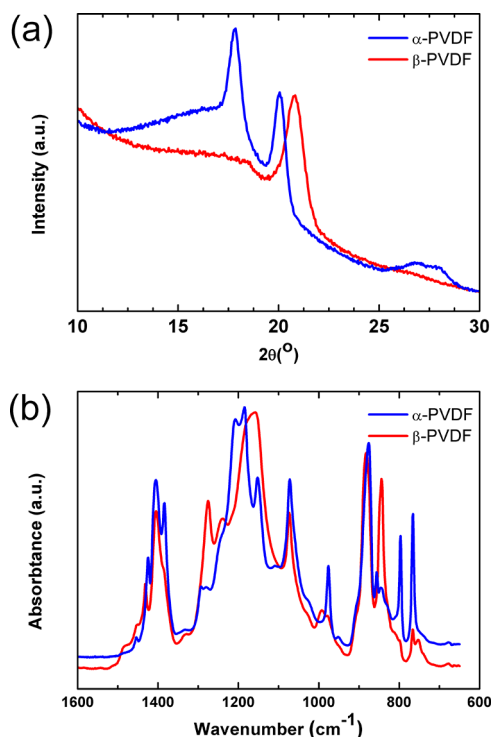

Figure 3. (a) Grazing incidence X-ray diffraction scans, and (b) corresponding FTIR spectra of thin PVDF:PMMA (70:30) films produced by wire bar coating from DMF, followed by melting at 200 °C for 2 h in vacuum. The slowly cooled blend film crystallizes in the α-phase, while the ice-quenched and annealed blend film forms the β-phase of PVDF.

Table 1. Percentage of PVDF β-Phase in PVDF:PMMA Blends As Calculated from FTIR Spectra[a]

M_w of PMMA, kg/mol	90:10	80:20	70:30
2	21	100	92
50	70	100	98
91	40	100	92

[a]The PVDF:PMMA compositions investigated were 90:10; 80:20 and 70:30. The blends were wire-bar coated from DMF, melted at 200 °C in vacuum, ice quenched and subsequently annealed for 2 h at 150 °C. The molecular weight, M_w, of PMMA was varied from 2 kg/mol, 50 kg/mol to 91 kg/mol.

suppressed, the spherulite size decreases to nanocrystalline, in agreement with the report by Kang et al.[17] At PMMA content above 40 wt % blend films remain amorphous. The microstructure hardly depends on the molecular weight of the PMMA. The surface roughness is presented in the inset of Figure 5 as a function of PMMA content. Ferroelectric films with an rms roughness less than 2 nm can be obtained.

4. MORPHOLOGY EVOLUTION FROM TIME-RESOLVED PHASE-FIELD SIMULATIONS

In the molten and amorphous vitreous state PVDF and PMMA are fully miscible. Phase separation in the PVDF:PMMA blend films occurs upon annealing. The driving force is the crystallization of the PVDF. To qualitatively understand the crystallization behavior and to explain the size and shape of the crystalline PVDF domains, as well as the redistribution of the amorphous PMMA, we performed time-resolved numerical
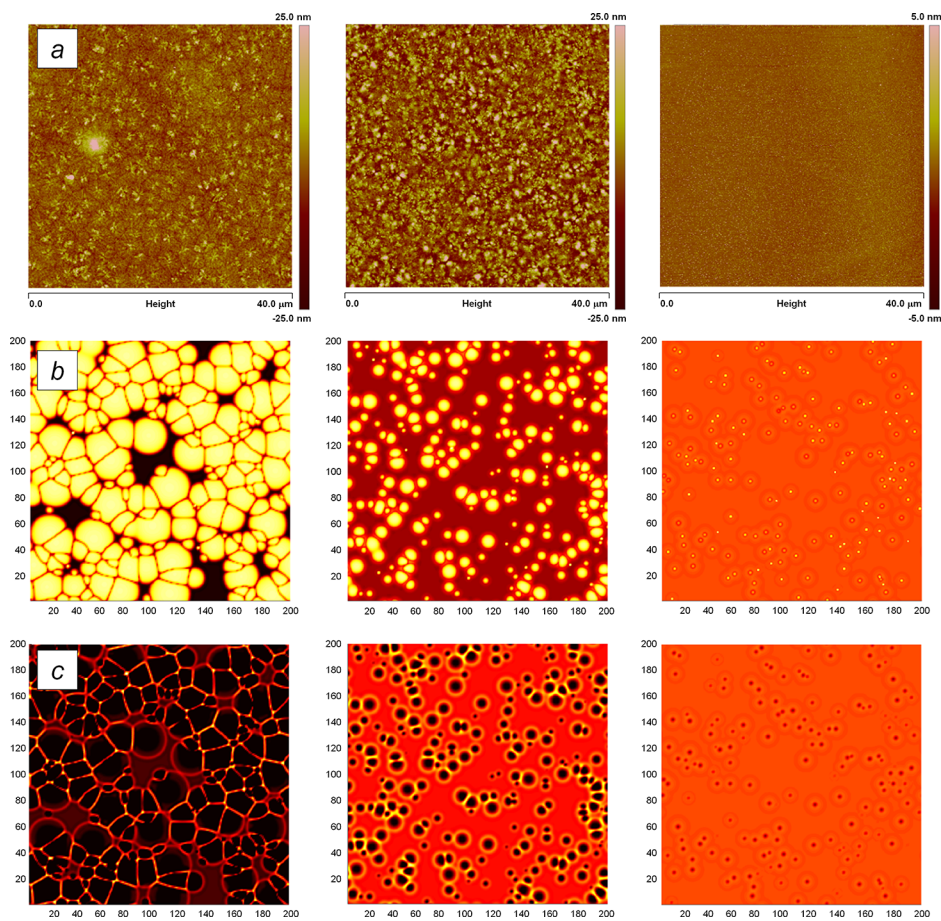
Figure 4. Solidification behavior of PVDF:PMMA blend thin films of compositions from left to right of 98:2, 90:10, and 70:30 (w/w): (a) AFM height profiles (40 μm × 40 μm); (b) PVDF crystallization (phase-field simulation on arbitrary length scale); (c) PMMA redistribution upon crystallization (phase-field simulation on arbitrary length scale). The displayed simulation results refer to PMMA with a molecular weight, M_w, of 91 kg/mol, but comparable images were obtained from 50 kg/mol and 2 kg/mol.
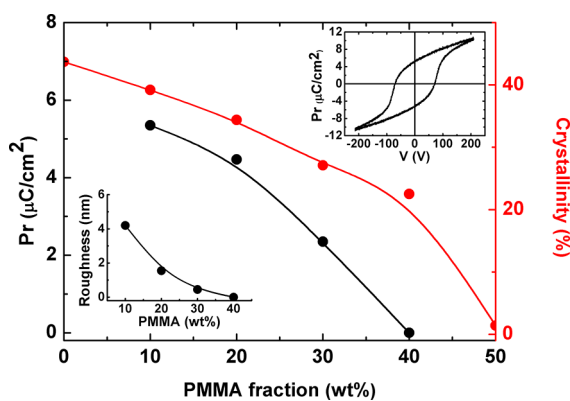

Figure 5. Ferroelectric phase diagram of PVDF:PMMA. Blend films were wire-bar coated from DMF, then molten at 200 °C in vacuum, ice quenched and subsequently annealed for 2 h at 150 °C. The black symbols present the remnant polarization, P_r, as a function of composition (left axis). The red symbols present the degree of crystallinity as derived from the DSC first heating scan. The insets show a ferroelectric displacement loop for a PVDF:PMMA 90:10 capacitor, and the rms roughness derived from AFM measurements as a function of composition. The solid lines are a guide to the eye.

simulations. The approach is based on the thermodynamically consistent phase-field model proposed by Boettinger et al.[31]

4.1. Methodology. A phase-field model is a mathematical model for solving interfacial problems. It has mainly been applied to solidification dynamics,[31] but it has also been applied to other phenomena such as viscous fingering,[32] fracture dynamics,[33] and vesicle dynamics.[34] The microstructure in a phase-field model is described by a set of order parameters, each of which is related to a specific phase or crystallographic orientation. The continuously varying order parameter, η, interpolates between the different phases defined by thermodynamic equilibrium. For a crystallizing material η is a nonconserved quantity interpolating between the amorphous and crystalline phases, respectively denoted as $\eta = 0$ and $\eta = 1$. The interfacial region between an amorphous and crystalline domain has a finite dimension represented by $0 < \eta < 1$. As a result, an interface has a diffuse and continuous nature. The advantage of this approach compared to sharp interface models is that it does not require definition of interfacial boundary conditions and keeping track of the spatial coordinates of the interfaces during structure evolution.

Morphology evolution upon crystallization and/or amorphous–amorphous demixing is a consequence of the minimization of the total free energy of the system. A suitable free energy functional for a (stable or instable) polymer blend from which one or more components may crystallize has been formulated by Boettinger et al.[31] Here we extend this single-phase-field free energy functional by defining multiple phase-fields in order to allow for development of crystal grain

boundaries, as suggested earlier by Chen for a single material undergoing an order−disorder transition.[35] The physical explanation for the formation of the grain boundaries is the orientation mismatch of the chain segments located at the interface between two crystalline grains. The total free energy functional (integrated over the volume) for an m-component blend for which the crystalline state is described by n phase-fields is thus written as:

$$F = \int dV \left[\sum_{i=1}^{m} w_i \varphi_i \sum_{i=1}^{n} \eta_i^2 (1 - \eta_i)^2 + \sum_{i=1}^{n} \sum_{j>i}^{n} v_{ij} \eta_i^2 \eta_j^2 \right.$$
$$+ f_c(\varphi_1, \varphi_2, ...\varphi_m) \sum_{i=1}^{n} p(\eta_i) + f_a(\varphi_1, \varphi_2, ...\varphi_m)$$
$$\left. [1 - \sum_{i=1}^{n} p(\eta_i)] + \frac{1}{2} \sum_{i=1}^{n} \alpha_i (\nabla \eta_i)^2 + \frac{1}{2} \sum_{i=1}^{m} \kappa_i (\nabla \varphi_i)^2 \right] \tag{1}$$

with φ_i representing the volume fractions of the blend components. The total free energy is minimized assuming incompressibility:

$$\sum_{i=1}^{n} \eta_i = 1 \text{ and } \sum_{i=1}^{m} \varphi_i = 1 \tag{2}$$

The six terms in the integrand of eq 1 respectively describe: (i) the energy barrier between the crystalline and amorphous states, (ii) the energy barrier between crystalline states, (iii) the free energy of the crystalline state, (iv) the free energy of the amorphous state, (v) the free energy associated with the formation of spatial gradients in the phase field parameter η, and (vi) the free energy associated with spatial gradients in the volume fraction, φ. The functions $f_c(\varphi_1, \varphi_2, ..., \varphi_m)$ and $f_a(\varphi_1, \varphi_2, ..., \varphi_m)$ represent the free energy contributions associated with the homogeneous crystalline and amorphous states, usually expressed in terms of the Flory−Huggins mixing free energy. The free energy contribution of the crystalline state (f_c) also contains the free energies of the neat crystalline components, expressed as functions of the latent heat of fusion (L) and the reduced temperature according to

$$f_c^0 \approx L \frac{T - T_m}{T_m} \tag{3}$$

where T_m is the melting temperature. The free energy of the pure amorphous components is set to zero; hence $f_c^0 < f_a^0$ for $T < T_m$, i.e. the crystalline state is energetically favored at temperatures below T_m. The prefactors w and v respectively denote the height of the energy barriers for crystallization and grain merging. As grain merging is "unphysical", v should be chosen sufficiently high. The parameters α and κ are the gradient energy coefficients, respectively associated with the crystalline fraction and volume fraction (α is not to be confused with the crystalline α-phase of PVDF). w and α are related to the free energy penalty due to the formation of amorphous−crystalline interfaces, and for that, have been related to their spatial dimensions, surface free energy, and degree of under-cooling.[36] The functions $p(\eta)$ interpolate between the amorphous and crystalline states, thus excluding coexistence of the pure phases at the same spatial coordinate.

Crystallization and concomitant material redistribution is induced by introducing nuclei, i.e., areas within the computational domain for which $\eta \sim 1$. The subsequent structure

evolution with time follows from minimization of the total free energy by allowing mobility to the blend components. The development of phase- and concentration fields is modeled by simultaneously solving the Cahn−Hilliard and Allen−Cahn equations given in eqs 4,5 for the independent phase- and volume fractions under the incompressibility constraint of eq 2.

$$\begin{cases} \dfrac{\partial \varphi_1}{\partial t} = \nabla \cdot M_{\varphi_1}(\varphi_1) \nabla \left(\dfrac{\partial F}{\partial \varphi_1} \right) + \zeta_{\varphi_1} \\[2mm] \dfrac{\partial \varphi_2}{\partial t} = \nabla \cdot M_{\varphi_2}(\varphi_2) \nabla \left(\dfrac{\partial F}{\partial \varphi_2} \right) + \zeta_{\varphi_2} \\[2mm] \vdots \\[2mm] \dfrac{\partial \varphi_{m-1}}{\partial t} = \nabla \cdot M_{\varphi_{m-1}}(\varphi_{m-1}) \nabla \left(\dfrac{\partial F}{\partial \varphi_{m-1}} \right) + \zeta_{\varphi_{m-1}} \end{cases} \tag{4}$$

$$\begin{cases} \dfrac{\partial \eta_1}{\partial t} = M_\eta(M_\varphi, \alpha) \left(\dfrac{\partial F}{\partial \eta_1} \right) \\[2mm] \dfrac{\partial \eta_2}{\partial t} = M_\eta(M_\varphi, \alpha) \left(\dfrac{\partial F}{\partial \eta_2} \right) \\[2mm] \vdots \\[2mm] \dfrac{\partial \eta_{n-1}}{\partial t} = M_\eta(M_\varphi, \alpha) \left(\dfrac{\partial F}{\partial \eta_{n-1}} \right) \end{cases} \tag{5}$$

Here, M_φ and M_η respectively denote the diffusive mobility of the (amorphous) blend components and the crystalline interface mobility, whereby the latter may be considered as a function of the interfacial tension (through α), the local volume fraction of crystallizing material, and M_φ.[37] This method assumes chain segments to join a growing crystal via "diffusive jumps" from the amorphous phase. ζ_φ represents small thermally induced density fluctuations which, in case of an immiscible blend, induce amorphous demixing. Their presence is taken into account by the model, but of no consequence to the morphology evolution of the PVDF:PMMA blends processed under the conditions described in this paper.

We follow a semiquantitative approach to defining the input for the model, by assigning established, estimated, or arbitrary (but consistent) values to molecular and physical parameters. Table 2 lists the input parameters relating to the bulk properties

Table 2. Physical Parameters of Material Bulk Properties Used as Input for the Phase-Field Simulations

N_{PVDF}	N_{PMMA}	T_m (K)	T (K)	L (J/cm³)	χ
700	227; 125; 5	453	413	199	−0.295

of the materials involved. The effective degrees of polymerization (N) of PVDF and PMMA were calculated based on the molecular weight data listed in Table 1, taking four repeat units as the approximate persistence length of a flexible polymer chain, and considering the monomeric segments of the two polymers to be of comparable size. The latent heat of fusion of crystalline PVDF was taken from the literature.[38] In this modeling study we are not concerned with defining different crystalline phases for PVDF. We consider only one crystalline phase with thermodynamic characteristics coarsely representative of the β-phase. The

processing temperature ($T = 413\ K$) is the annealing temperature of the ice quenched amorphous layers. The lower critical solution temperature (LCST) bahavior of the PVDF:PMMA blend is characterized by a negative Flory–Huggins interaction parameter. In our simulations we adopt a value of χ of -0.295, as determined for 160 °C by Nishi and Wang.[21]

The assignment of w, α, and κ is less straightforward, as (experimental) physical data on gradient energy coefficients are scarce and often lacking. Furthermore, the usual definitions for κ based on the random phase approximation[39−41] cannot be used, as they assume the components being at least partially immiscible. Hence, although inspired on physical data applied previously in phase-field simulations of blends of organic materials,[42] their attribution is essentially arbitrary. Nevertheless, the parameters were treated in a fully consistent manner, thus allowing internal comparison between simulations performed for different PVDF:PMMA ratios. The spatial characteristics of α and κ, together with all simulation length and time scales, were made dimensionless by defining a characteristic length, λ, and a time, τ. Table 3 lists the dimensionless and arbitrary input parameters.

Table 3. Physical Parameters of Interfacial Properties and Material Motion, Used as Input for the Phase-Field Simulations

w (J/cm^3)	α/λ^2 (J/cm^3)	κ/λ^2 (J/cm^3)	$D\tau/\lambda^2$
40	50	20	1600

4.2. Simulation of Crystallization. Row a in Figure 4 shows the experimentally observed morphology of PVDF:PMMA blend films with composition ratios of 98:2, 90:10, and 70:30. Rows b and c present the corresponding morphology as obtained from the 2D numerical phase-field simulations. PMMAs of all three molecular weights yielded very comparable morphologies, in agreement with experimental observations. For this reason, only the results obtained for a molecular weight of 91 kg/mol, corresponding to N_{PMMA} of 227, are shown. In Figure 4, rows b and c, respectively, show the regions of crystalline PVDF and amorphous PMMA as a function of spatial coordinates. All simulations started from a homogeneous amorphous situation, running for the same number of cycles ($n \approx 30.000$) and using the same arbitrary nucleation attempt probability for each time step. The results, although representing a simplified version of physical reality, quantitatively reproduce the crystallization behavior of PVDF as a function of PMMA content: the largest crystalline fraction is observed for the 98:2 PVDF:PMMA blend and virtually no crystallization is observed for mixture of a PMMA content of ~30 wt %.

As the nucleation probability per time step is equal for all simulations, the decrease in crystallinity with PMMA content in the simulated blends is a result of a decrease in the growth rate of the crystals.[43] Consequently, it takes longer, and eventually too long, for the growing crystals to become sufficiently large to prevent the nucleus form "re-dissolving" into the amorphous blend. In other words, at a high PMMA fraction the free energy gain per time step as a result of crystal growth becomes too small to overcompensate for the penalty associated with the formation of interface regions around the nucleus. In blends of an intermediate PMMA fraction (i.e., the 90:10 blend) nucleation is still successful but the growth is retarded due to a decrease in interface mobility and flux of amorphous PVDF material toward the crystalline interface. Crystal growth is also thermodynami-

cally retarded due to the formation of pronounced gradients in the amorphous PMMA regions surrounding the spherulites. These effects explain the decrease in growth rate at PVDF:PMMA ratio's for which the crystallization temperature of the β-phase is still considerably higher than the glass transition temperature (see phase diagram in Figure 2). Naturally, for a blend with a very high PMMA fraction (e.g., 40 wt %) crystallization will be further hindered by kinetic effects associated with the increase of the glass transition temperature of the blend, which is not considered by the simulations as polymer chain mobility is kept constant.

We further note that the tightly connected spherulitic grain morphology of the crystalline regions observed for the 98:2 blend (row a, left) is reproduced by the corresponding simulation (row b, left). The morphology is characterized by relatively sharp angles between the grain boundaries, despite the formation of PMMA enriched regions between the grains due to expulsion and accumulation in the boundary regions (row c). The simulation of the behavior of the 90:10 blend shows that a higher PMMA content may cause the grain boundary angles to become more "rounded", if more material is expelled and accumulated during spherulite growth (cf. row c, middle).

5. FERROELECTRICITY OF PVDF:PMMA BLEND FILMS

The displacement current of PVDF:PMMA blend films as a function of bias voltage was measured in capacitors. A typical hysteresis loop for a thin film capacitor of a PVDF:PMMA (90:10) blend is shown in the inset of Figure 5. Contrary to the P(VDF−TrFE) copolymer which always displayed a square loop, for the blend films always slim hysteresis loops were recorded, irrespective of the experimental conditions such as applied voltage and number of cycles. As leakage currents could be ruled out, we attribute this response to their nanocrystalline microstructure. The coercive field is about 110 MV/m, comparable to that reported for PVDF,[44] and higher than that reported for the ferroelectric P(VDF−TrFE). The remnant polarization is presented as a function of PMMA content in Figure 5. The polarization decreases with PMMA content from 5.4 μC/cm^2 at 10 wt % PMMA to a negligible polarization at 40 wt % PMMA.

The polarization depends on the annealing temperature after ice quenching. We investigated blend films after ice quenching annealed at a low temperature of only 120 °C. According to XRD measurements the PVDF still crystallized in the ferroelectric β-phase, but the degree of crystallinity of the films was low. Pristine capacitors were not ferroelectric. A propeller-like slim paraelectric loop was observed. A remnant polarization up to 5 μC/cm^2 for PVDF:PMMA 90:10 could, however, be induced at elevated temperature, around 100 °C, by repeated cycling at voltages far above the coercive field. The polarization is not permanent but disappears upon cooling down to room temperature. The origin therefore is different than for the recently reported electric-field induced polarization of ultrathin films of P(VDF−TrFE).[45] XRD measurements have demonstrated that for those films the changes are permanent and due to electric-field induced crystallization.

The dependence of the remnant polarization on PMMA content in the blend films is plotted in Figure 5 together with the degree of the crystallinity as calculated from the enthalpy of fusion deduced from thermal analysis; see Experimental Section. Neat PVDF is a semicrystalline polymer for which we calculated a degree of crystallinity of 45%. The crystallinity monotonically decreases with increasing PMMA content. At 40 wt % PMMA and above content, the crystallinity is negligible; i.e., these blend

films are essentially amorphous. The crystallization is kinetically hampered as the crystallization temperature approaches the glass transition temperature, as can be seen in the phase diagram (Figure 2). Comparable values for the crystallinity as a function of PMMA content have been reported previously.[38,46,47] The remnant polarization is due to a permanent induced surface charge density. Not surprisingly, therefore, Figure 5 shows that the remnant polarization of the PVDF:PMMA unambiguously scales with the crystallinity. A similar relation has been reported for blend films of P(VDF−TrFE) with PMMA[48] albeit that the change in entropy was plotted rather than degree of crystallinity.

Considering the apparently high transition temperatures observed in our thermal analysis, we set out to investigate the thermal stability of blend-capacitors. The remnant polarization and coercive field are presented as a function of temperature in Figure 6 for three PVDF:PMMA blend ratios of 90:10, 80:20,
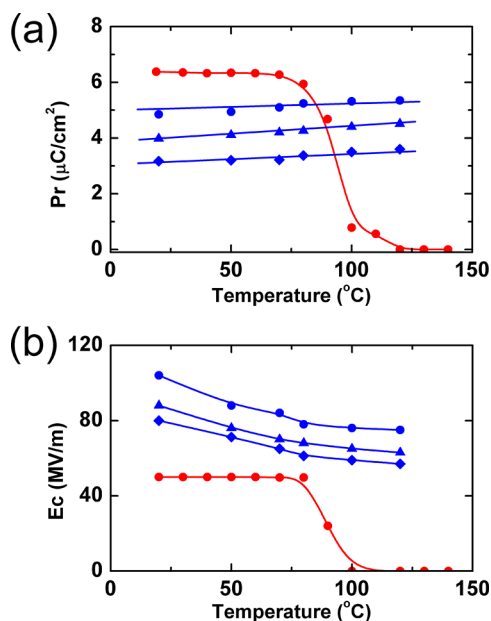

Figure 6. Temperature budget. Remnant polarization, P_r (a), and the corresponding coercive field, E_c (b), as a function of temperature. In blue are the measurements for PVDF:PMMA blends with compositions of 90:10 (●), 80:20 (▲), and 70:30 (♦) wt %. The films were wirebar coated from DMF, melted at 200 °C in vacuum, ice quenched, and subsequently annealed for 2 h at 150 °C. The red dots represent measurements on the copolymer P(VDF−TrFE). The solid lines are a guide to the eye.

and 70:30. Interestingly, for all blends the polarization is constant up to 120 °C. As a matter of fact, it very slightly increases. The coercive field decreases with temperature. The activation energy is in the order of 10 meV. For comparison data of the polarization as a function of temperature for the copolymer P(VDF−TrFE) as taken from Figure 1 are included as well. The polarization of PVDF:PMMA is much more stable than that of P(VDF−TrFE). The thermal stability is directly related to the Curie temperature. The ferroelectric to paraelectric phase transition of P(VDF−TrFE) occurs around 100 °C. The phase diagram of Figure 2 indicates that this transition temperature in PVDF:PMMA blends is much higher, even above the melting temperature of β-PVDF. As a consequence, above about 80 °C PVDF:PMMA blends outperform the copolymer P(VDF−TrFE).

6. SUMMARY AND CONCLUSION

Here we have investigated the ferroelectric phase diagram of PVDF:PMMA. To this end, we first determined the binary nonequilibrium temperature/composition diagram by DSC measurements. The melting point and glass transition temperature monotonically change with composition, which reconfirms that the two polymers are fully miscible in the melt over the whole composition range. In PVDF:PMMA blends films, made from solution or melt, PVDF crystallizes in the paraelectric α-phase. However, when the blend films were molten, ice quenched, and subsequently annealed close to its melting temperature, PVDF crystallizes in the ferroelectric β-phase. PMMA promotes formation of the β-phase over the α-phase for steric reasons; the dipole/dipole interactions favor the trans−trans conformation of the highly polar β-PVDF over the trans−gauche conformation of the nonpolar α-PVDF.

The presence of PMMA suppresses the crystallization of PVDF and, hence, the roughness of blend films notably decreases with increasing PMMA content. Above 40 wt % PMMA, the films are amorphous. The crystallization is then kinetically hampered as evidenced in the phase diagram by the crystallization temperature being close to the glass transition temperature. Phase-field simulations of the crystallization of PVDF from the miscible vitreous blends show that crystal growth at high PMMA fractions is retarded thermodynamically due the formation of gradients in the amorphous polymer regions with associated free energy penalty. The simulations further show that the PMMA content may also influence the shape of the PVDF spherulites due to expulsion and accumulation of PMMA toward the crystal grain boundaries.

The remnant polarization decreases with increasing PMMA content from 5.5 μF/cm^2 at 10 wt % to negligible values at 40 wt %. We have shown that the polarization unambiguously scales with the degree of crystallinity of the PVDF. The thermal stability of the polarization is directly related to the Curie temperature, which for the PVDF:PMMA blends is higher than the melting temperature of β-PVDF. Hence above 100 °C, the PVDF:PMMA blends outperform the standard copolymer P(VDF−TrFE), which renders these blends ideal candidates for applications that require high operating temperatures.

■ EXPERIMENTAL SECTION

Materials and Film Preparation. The random copolymer of P(VDF−TrFE) (65−35 mol %) was purchased from Solvay. PVDF (M_w 180 kg/mol) and PMMA (M_w 2, 50, and 91 kg/mol), were purchased from Sigma-Aldrich. All materials were used as received. The solubility of PVDF in a number of solvents as well as the Hansen solubility parameters extracted have been reported.[49] PVDF has a limited solubility in common organic solvents as alcohols, chlorinated solvents and acids. Good solvents are, e.g., N,N-dimethylformamide (DMF), dimethyl sulfoxide and N-methyl-2-pyrrolidone. We prepared blend solutions by codissolving PVDF and PMMA in DMF, typically 10% by weight total solids. Thin films were prepared by wire-bar (Meyer rod) coating with a K202 control coater (RK Print) at 50 °C. Meyer rod-coating is well-established technique used in the coating industry to make liquid thin films in a continuous and controlled manner.[50] After coating the films were molten at 200 °C for 2 h in a vacuum oven, followed by quenching in ice water to achieve an amorphous state. A subsequent annealing step of 140−150 °C close to the melting temperature of PVDF was then applied to achieve the ferroelectric β-phase.

Thin Film Characterization. Differential scanning calorimetry (DSC) was conducted under N$_2$ atmosphere, on as-cast films, at a scan rate of 10 °C/min, with a Mettler Toledo DSC 822e instrument. The degree of crystallinity was calculated using ΔH_{fusion} for neat PVDF of

102.5 J/g.[51] The glass transition temperature was determined employing Mettler-Toledo Stare software version 9.1. The nonequilibrium composition/temperature phase diagram was established with those thermal analysis data: melting and crystallizing transitions were deduced from the peak maxima of the corresponding endo- and exotherm in the respective thermograms. Glass transition temperatures were taken to be the inflection points. The film thickness was measured with a Dektak profilometer. The surface morphology of the films was characterized by atomic force microscopy (AFM) (Nanoscope Dimension 3100 Bruker). To ascertain the crystal phases of the films, both grazing incidence X-ray diffraction (XRD) and Fourier-transform infrared spectroscopy (FTIR) were used. XRD scans were obtained with a Philips X'pert MPD diffractometer, using the line focus of a Cu-anode X-ray tube. For the grazing incidence setup we used a divergence slit of 0.03° and a parallel plate collimator in front of the detector. The incidence angle was fixed during the measurement at an angle of 0.23° just above the critical angle of total diffraction. Infrared spectra of crystallized PVDF:PMMA blends were recorded using a Bruker Vertex spectrometer attached to a Hyperion FT-IR microscope. The scans were performed with a resolution of 4 cm^{-1}. For a sample containing both α- and β-polymorph PVDF, the relative fraction of α-phase, $F(\alpha)$, was calculated by a method proposed by Gregorio and Cestari.[52] On the basis of Lambert–Beer, $F(\alpha)$ is given by

$$F(\alpha) = \frac{X_\alpha}{X_\alpha + X_\beta} = \frac{A_\alpha}{A_\alpha + (K_\alpha C_\alpha / K_\beta C_\beta) A_\beta} = \frac{A_\alpha}{A_\alpha + 0.8 A_\beta}$$

(6)

for a sample with average total monomer concentration C of 0.0305 mol/cm^3. X is the degree of crystallinity of the α- or β-phase. A_α and A_β refer to the absorbencies at 763 and 840 cm^{-1}, respectively, associated with the α- and β-phases. K represents the absorbances at the corresponding wavenumber; K_α is 6.1×10^4 cm^2 mol^{-1} and K_β is 7.7×10^4 cm^2 mol^{-1}.

Device Fabrication and Characterization. Capacitors were fabricated on thermally oxidized silicon monitor wafers on which 50 nm thick Au bottom electrodes on a 2 nm Ti adhesion layer were photolithographically defined. The blend films were applied and annealed. Au was evaporated through a shadow mask and used as top electrode. The device area varied from 0.059 to 1.38 mm^2. Electric displacement loops versus electric field for the capacitors were measured using a Sawyer–Tower circuit, consisting of a Tektronix AFG3102 function generator, a TektronixTDS3032B oscilloscope and a Krohn-Hite 7600 wide band amplifier. The capacitors were measured with a continuous triangular wave signal, to reduce the time at maximum bias, at a frequency of 100 Hz and using a reference capacitor of 216 nF.

■ **AUTHOR INFORMATION**

Corresponding Author
*E-mail: mengyuan.li@rug.nl.
Notes
The authors declare no competing financial interest.

■ **ACKNOWLEDGMENTS**

■ **REFERENCES**

(1) Scott, J. F., *Ferroelectric Memories*: Springer-Verlag: Berlin, 2000.
(2) Naber, R. C. G.; Asadi, K.; Blom, P. W. M.; de Leeuw, D. M.; de Boer, B. *Adv. Mater.* **2010**, *22*, 933.
(3) Naber, R. C. G.; Tanase, C.; Blom, P. W. M.; Gelinck, G. H.; Marsman, A. W.; Touwslager, F. J.; Setayesh, S.; de Leeuw, D. M. *Nat. Mater.* **2005**, *4*, 243.
(4) Khan, M. A.; Bhansali, U. S.; Alshareef, H. N. *Adv. Mater.* **2012**, *24*, 2165.
(5) Asadi, K.; de Leeuw, D. M.; de Boer, B.; Blom, P. W. M. *Nat. Mater.* **2008**, *2*, 547.
(6) Asadi, K.; Li, M.; Stingelin, N.; Blom, P. W. M.; de Leeuw, D. M. *Appl. Phys. Lett.* **2010**, *97*, 193308.
(7) Asadi, K.; Li, M.; Blom, P. W. M.; Kemerink, M.; de Leeuw, D. M. *Mater. Today* **2011**, *14*, 592.
(8) Li, M.; Stingelin, N.; Michels, J. J.; Spijkman, M.; Asadi, K.; Beerends, R.; Biscarini, F.; Blom, P. W. M.; de Leeuw, D. M. *Adv. Funct. Mat.* **2012**, *22*, 2750.
(9) Hu, Z.; Tian, M.; Nysten, B.; Jonas, A. M. *Nat. Mater.* **2009**, *8*, 62.
(10) Lovinger, A. J. *Science* **1983**, *220*, 1115.
(11) Furukawa, T. *Adv. Colloid Interface Sci.* **1997**, *183*, 71.
(12) Park, Y. J.; Bae, I.; Kang, S. J.; Chang, J.; Park, C. *IEEE Trans. Dielectr. Electr. Insul.* **2010**, *17*, 1135.
(13) Xu, H.; Zhong, J.; Liu, X.; Chen, J.; Shen, D. *Appl. Phys. Lett.* **2007**, *90*, 092903.
(14) Zhang, Q. M.; Bharti, V.; Zhao, X. *Science* **1998**, *280*, 2101.
(15) Ma, W.; Zhang, J.; Chen, S.; Wang, X. *Appl. Surf. Sci.* **2008**, *254*, 5635.
(16) Sun, J.; Yao, L.; Zhao, Q.; Huang, J.; Song, R.; Ma, Z.; He, L.; Huang, W.; Hao, Y. *Front. Mater. Sci.* **2011**, *5*, 388.
(17) Kang, S. J.; Park, Y. J.; Bae, I.; Kim, K. J.; Kim, H. C.; Bauer, S.; Thomas, E. L.; Park, C. *Adv. Funct. Mater.* **2009**, *19*, 2812.
(18) Roerdink, E.; Challa, G. *Polymer* **1980**, *21*, 509.
(19) Belke, R. E.; Cabasso, I. *Polymer* **1988**, *29*, 183.
(20) Juncknickel, B.-J., *Ferroelectric Polymers*: Marcel Dekker: New York, 1995.
(21) Nishi, T.; Wang, T. T. *Macromolecules* **1975**, *8*, 909.
(22) Yang, D. C.; Thomas, E. L. *J. Mater. Sci. Lett.* **1984**, *3*, 929.
(23) Yang, D. C.; Thomas, E. L. *J. Mater. Sci. Lett.* **1987**, *6*, 593.
(24) Hourston, D. J.; Hughes, I. D. *Polymer* **1977**, *18*, 1175.
(25) Peterlin, A.; Houlbrook, J. *J. Mater. Sci.* **1967**, *2*, 1.
(26) Teyssedre, G.; Bernes, A.; Lacabanne, C. *J. Polym. Sci., Part B: Polym. Phys.* **1993**, *31*, 2027.
(27) Tashiro, K.; Takano, K.; Kobayashi, M.; Chatani, Y.; Tadokoro, H. *Polymer* **1983**, *24*, 199.
(28) Gregorio, R., Jr. *J. Appl. Polym. Sci.* **2006**, *4*, 3272.
(29) Kim, K. J.; Cho, Y. J.; Kim, Y. H. *Vibr. Spectrosc.* **1995**, *9*, 147.
(30) Braun, D.; Jakobs, M.; Hellmann, G. P. *Polymer* **1994**, *35*, 706.
(31) Boettinger, W. J.; Warren, J. A.; Beckermann, C.; Karma, A. *Annu. Rev. Mater. Res.* **2002**, *32*, 163.
(32) Folch, R.; Casademunt, J.; Hernández-Machado, A.; Ramírez-Piscina, L. *Phys. Rev. E* **1999**, *60*, 1734.
(33) Karma, A.; Kessler, D. A.; Levine, H. *Phys. Rev. Lett.* **2001**, *87*, 045501.
(34) Biben, T.; Kassner, K.; Misbah, C. *Phys. Rev. E* **2005**, *72*, 041921.
(35) Chen, L-. Q. *Scr. Metall. Mater.* **1995**, *32*, 115.
(36) Wheeler, A. A.; Boettinger, W. J.; McFadden, G. B. *Phys. Rev. A* **1992**, *45*, 7424.
(37) Warren, J.; Boettinger, W. *Acta Metall. Mater.* **1995**, *43*, 689.
(38) Morra, B. S.; Stein, R. S. *J. Polym. Sci., Polym. Phys. Ed.* **1982**, *20*, 2243.
(39) P. G. de Gennes, *Scaling Concepts in Polymer Physics*; Cornell University Press: Ithaca, NY, 1979.
(40) Binder, K. *J. Chem. Phys.* **1983**, *79*, 6387.
(41) Roe, R. J. *Macromolecules* **1986**, *19*, 728.
(42) Saylor, D. M.; Kim, C. S.; Patwardhan, D. V.; Warren, J. A. *Acta Biomater.* **2007**, *3*, 851.
(43) This does, however, not nullify the influence of PMMA content on the physical nucleation rate, but it is not considered here.
(44) Kepler, R. G. *Org. Coat. Plast. Chem.* **1978**, *38*, 706.
(45) Nakajima, T.; Mabuchi, Y.; Morimoto, T.; Furukawa, T.; Okamura, S. *IEEE* **2011**, 978−1-4577−1025−4/11.

(46) Schaffner, F.; Wellscheid, R.; Jungnickel, B.-J. *IEEE Trans. Elect. Insul.* **1991**, *26*, 78.

(47) Hahn, B. R.; Herrmann-Schonherr, O.; Wendorff, J. H. *Polymer* **1987**, *28*, 201.

(48) Moreira, R. L.; Faria, L. O.; Marini, G.; Wisniewski, C.; Giacometti, J. A. *Ferroelectrics* **2002**, *268*, 101.

(49) Bowino, A.; Capannelli, G.; Munari, S.; Turturro, A. *J. Polym. Sci., Part B: Polym. Phys.* **1988**, *26*, 785.

(50) MacLeod, D. M. in Coatings Technology: Fundamentals, *Testing and Processing Technique*; Tracton, A.A., Ed.; CRC Press: Boca Raton, FL, 2007; Chapter 19

(51) Mead, W. T.; Zachariades, A. E.; Shimada, T.; Porter, R. S. *Macromolecules* **1979**, *12*, 473.

(52) Gregorio, R., Jr.; Cestari, M. *J. Polym. Sci., Part B: Polym. Phys.* **1994**, *32*, 859.